Accepted Manuscript

Multi-component topology and material orientation design of composite structures (MTO-C)

Yuqing Zhou, Tsuyoshi Nomura, Kazuhiro Saitou

PII: S0045-7825(18)30383-9
DOI: https://doi.org/10.1016/j.cma.2018.07.039
Reference: CMA 12011

To appear in: *Comput. Methods Appl. Mech. Engrg.*

Received date : 30 March 2018
Revised date : 22 June 2018
Accepted date : 31 July 2018

Please cite this article as: Y. Zhou, T. Nomura, K. Saitou, Multi-component topology and material orientation design of composite structures (MTO-C), *Comput. Methods Appl. Mech. Engrg.* (2018), https://doi.org/10.1016/j.cma.2018.07.039

Multi-component topology and material orientation design of composite structures (MTO-C)

Yuqing Zhou[a], Tsuyoshi Nomura[b,c], Kazuhiro Saitou[a]

[a] *University of Michigan, 2350 Hayward, Ann Arbor, Michigan, 48109, USA*
[b] *Toyota Research Institute of North America, 1555 Woodridge Avenue, Ann Arbor, Michigan, 48105, USA*
[c] *Toyota Central R & D Labs., Inc., 41-1 Yokomichi, Nagakute 480-1192, Japan*

Abstract

This paper presents a topology optimization method for structures made of multiple composite components (substructures) with tailored material orientations. It is capable of simultaneously optimizing the overall topology, component partitioning, and material orientation for each component, via a vector field variable that specifies fractional membership to each component, together with the conventional density and orientation variables. The convergence towards the non-fractional, zero/one membership during optimization is achieved by a hypercube-to-simplex projection of the membership variables with a penalization scheme. Through the integration with a continuous material orientation design method, the proposed method is capable of generating multi-component composite structures with tailored material orientations for each component, without a prescribed set of alternative discrete angles. The new method extends the existing continuous material orientation design methods by introducing the concept of components (substructures) with the component-level orientation control, which is suitable for economical production with the conventional high-volume composite manufacturing processes.

Keywords: Topology optimization, Multi-component structures, Composite materials, Material orientation design

1. Introduction

Recent societal demand for energy saving has prompted increased emphasis on lightweighting in structural design. While the utilization of fiber

reinforced composite materials can dramatically cut down structural weight, a significant trade-off exists between the production cost and structural performance. Variable axial composite (VAC) is a class of composite materials reinforced by long fibers with varying orientations, produced by advanced manufacturing processes such as automated tape layout (ATL), tailored fiber placement (TFP), and continuous fiber printing (CFP). Generally speaking, manufacturing processes with higher freedom in orientation control can produce higher performing composites, but cost more than those with lower freedom in orientation control. For this reason, the conventional fixed-axis composites, despite their inferior performance, are widely adopted in many commercial applications, especially for large-scale and mass-produced structural products. Figure 1 shows a comparison of typical composite manufacturing processes in terms of their freedom in fiber orientation control and suitability for economical production in large quantities. The injection molding of resins mixed with short fibers, also known as short fiber injection molding (SFIM), is included as a baseline benchmark, which approximately performs as isotropic materials due to random and discontinuous fiber orientations.

Motivated by the recent advent of composite manufacturing processes, much effort has been made to develop topology optimization methods for designing anisotropic material orientations. Based on their mathematical formulations, the existing methods can be categorized into two major classes: the discrete orientation method and the continuous orientation method.

The first class optimizes the material orientations among a prescribed set of alternative discrete angles, hence termed the discrete orientation method. Such prescribed discrete angles are often preferred in aerospace and wind turbine industries for manufacturability reasons (Sørensen and Lund (2013); Kennedy and Martins (2013)). Haftka and colleagues developed discrete optimization formulations for selecting fiber orientation angles from a prescribed, discrete set, *e.g.*, $\{0°, 45°, 90°, 135°\}$ (Le Riche and Haftka (1993); Nagendra et al. (1996); Liu et al. (2000); Haftka and Gürdal (2012)), which were solved using genetic algorithms. These non-gradient methods received criticisms on their applicability to the continuum topology optimization due to the computational effort involved when solving problems with a large number of design variables (Rozvany (2009); Sigmund (2011)). To enable the sensitivity analysis and the efficient gradient optimization, Lund and colleagues proposed the discrete material optimization (DMO) approach (Stegmann and Lund (2005); Niu et al. (2010); Sørensen et al. (2014)), which relaxed the orig-

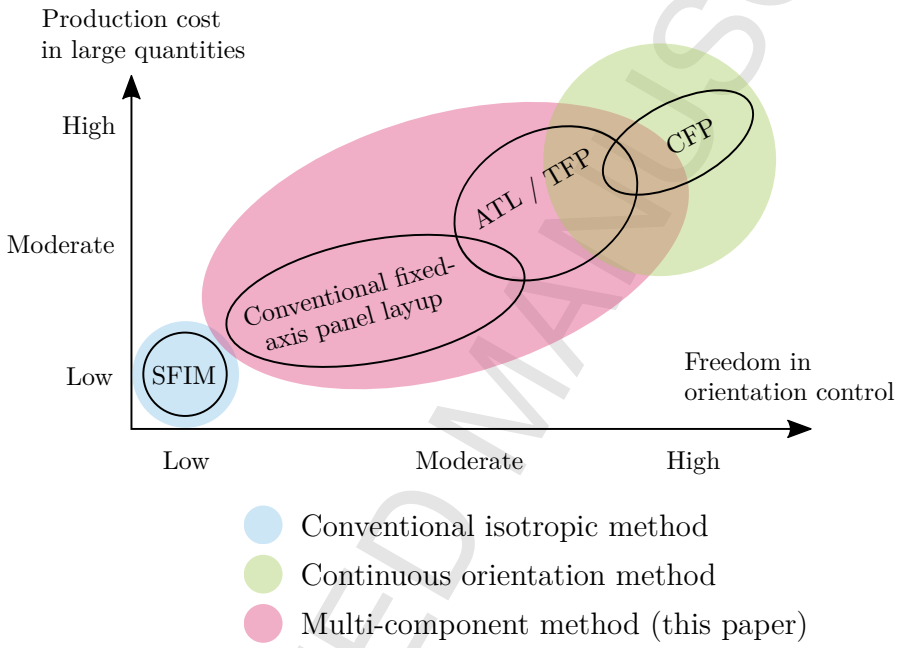

Figure 1: A qualitative comparison of different composite manufacturing processes in terms of the production cost in large quantities (vertical axis) and freedom in orientation control (horizontal axis). As a manufacturing process becomes more economical for mass production, it sacrifices freedom in controlling fiber orientations. The suitability of different topology design methods is also plotted. (SFIM: short fiber injection molding; ATL: automated tape layout; TFP: tailored fiber placement; CFP: continuous fiber printing)

inal combinatorial problem to a continuous optimization problem through material tensor aggregation and penalization. Thanks to efficient gradient optimization, the prescribed set of alternative discrete angles can be of a larger size, but it remains as an input to the optimization. Other variations following the DMO concept have also been developed, *e.g.*, the shape function with penalization method (Bruyneel (2011)) and its generalization to more choices of alternative discrete angles (Gao et al. (2012)), and the peak function approach (Kiyono et al. (2017)). By introducing additional unity constraints on the sum of the fractional selections of alternative angles, other formulations (Hvejsel and Lund (2011); Kennedy and Martins (2013)) have been proposed as alternatives to the DMO formulation. A large number of unity constraints associated with these formulations, however, imposes challenges on optimization solvers in large-scale problems.

Despite its popularity and intuitive formulation, these discrete orientation methods suffer from a common issue: the need of a prescribed set of alternative discrete angles as an input. While, in theory, a set of infinitely large number of alternative discrete angles can contain the true optimal angles, the methods are limited to find the best angles only among the given alternatives, which may well be suboptimal. In addition, while some extensions intend to address the selection of different angles for each substructure (typical for multi-panel construction of composite structures), the boundaries between substructures are simply determined by the prescribed division of the design domain, typically squares, without optimization processes.

The second class optimizes the material orientation within a continuous range of angles, not among alternative discrete angles, hence termed the continuous orientation method. Pedersen (1989, 1991) used an analytical method and the optimality criteria to find the optimal local orientations that also avoided convergence to the local minima. Bruyneel and Fleury (2002) and Lindgaard and Lund (2011) proposed the continuous fiber angle optimization (CFAO) method where the orientation angles are regarded as continuous design variables that can take range $[0, 2\pi]$. While intuitive, this angular representation suffers from the convergence to the local minima due to the periodic nature of material properties with respect to the orientation angles. To overcome this issue, Nomura et al. (2015) proposed the use of Cartesian components of the orientation vector as design variables combined with an isoparametric projection, and empirically demonstrated superior convergence behaviors.

Shown also in Figure 1 is the suitability of different topology optimiza-

tion methods for designing structures with anisotropic material orientations. Structures designed by the continuous orientation methods are most suitable for production by the manufacturing processes with the highest freedom in orientation control, *e.g.*, CFP. On the other hand, structures designed by the conventional isotropic topology optimization methods, *e.g.*, SIMP method (Bendsøe (1989); Rozvany et al. (1992)), are well suited for production by the manufacturing processes at the lowest end of orientation control and cost, *e.g.*, SFIM, since materials perform almost as isotropic materials. In between these extreme is a space for the manufacturing processes with moderate orientation control and cost, *e.g.*, conventional layup of fixed-axis composite panels, TFP, and ATL. Fixed-axis composite layup process is an economical composite manufacturing process that has been commonly adopted in serial production industries, *e.g.*, automotive. The economical mass production is achieved by utilizing fixed-axis bulk composite panels. Some degree of structural performance tuning is realized by the layup of several pieces of fixed-axis composite panels in different locations of a larger mold prior to the resin injection and curing process. The final detailed part profile is then cut out via waterjet cutting.

Structural designs suitable for production by these processes with moderate orientation control and cost should be made of a relatively small number of distinct substructures (components), each of which has a single material orientation, possibly with small variations for TFP and ATL, tailored for overall structural performances. As discussed above, the existing discrete orientation methods come short for this purpose due to their requirement of a prescribed set of alternative discrete angles, while the manufacturing processes are capable for tailoring material orientations within each component. The method proposed in this paper intends to fill this gap.

The multi-component topology optimization (MTO) is a generalization of the conventional monolithic (single-piece) topology optimization. From a viewpoint of mathematical formulation, it is closely related to multi-material topology optimization (*e.g.*, Thomsen (1992); Sigmund and Torquato (1997); Sigmund (2001); Wang and Wang (2004); Stegmann and Lund (2005); Zuo and Saitou (2017); Da et al. (2017); Liu and Ma (2018)), where different materials in multi-material structures can be regarded as different components in multi-component structures. Unlike most topology optimization studies including multi-material topology optimization that focus merely on optimizing various structural performances, MTO is motivated by the need of generating ready-to-manufacture optimal structures made as assemblies of

multiple components, each of which conforms geometric constraints imposed by a chosen manufacturing process. It was originally formulated as discrete optimization problems and solved by genetic algorithms (Lyu and Saitou (2005); Yildiz and Saitou (2011); Guirguis et al. (2015)). Zhou and Saitou (2018) recently proposed a continuously relaxed formulation of MTO, which enabled the use of efficient gradient optimization algorithms. This gradient-based MTO framework has also been applied to designing structures assembled from components produced by additive manufacturing (Zhou and Saitou (2017)).

In this paper, we propose a topology optimization method for structures made of multiple composite component (substructures) with tailored material orientations. Through the integration of a continuous material orientation design method within the MTO framework, the proposed method is capable of generating multi-component composite structures with tailored material orientations for each component, without a prescribed set of alternative discrete angles. The resolution of the material orientation for each component can be controlled seamlessly from unidirectional to curvilinear and to general variable axis by changing an allowable variation. The new method extends the continuous material orientation design methods by introducing the concept of components (substructures) with the component-level orientation control, which is suitable for economical production with the conventional high-volume composite manufacturing processes.

The remainder of this paper is organized as follows. Section 2 presents the problem formulation. The minimum compliance problems with in-plane loading configurations are chosen as numerical examples, and are presented in Section 3. Finally, Section 4 summarizes the current study and discusses opportunities for future research.

2. Formulation

This section presents the problem formulation for the simultaneous multi-component topology and material orientation design. First, the design fields are defined for material density, material orientation, and component membership, followed by a SIMP-like formulation of multi-component elasticity tensor composition through the component membership field. Finally, the overall optimization problem is presented.

2.1. Design fields

As illustrated in Figure 2, there are three layers of design fields for the proposed multi-component topology and material orientation design problem. The first layer contains the density field ρ as a common field for all components, which represents the material density of each design point, *i.e.*, the overall topology of a structure. The second layer contains the component membership field $m^{(k)}$, which represents the fractional membership of each design point to component k, where $k = 1, 2, \cdots, K$ and K is the prescribed, maximum allowable number of components. The third layer contains the material orientation field $\vartheta^{(k)} = (\varsigma^{(k)}, \zeta^{(k)})$, a Cartesian vector representing the orientation of each design point in component k. Depending on the radius of the regularization filter applied to the material orientation field, the resulting material orientation for each component can either be unidirectional or curvilinear. Details discussion for the density, component membership, and material orientation design fields are presented in following sections. The regularizations of these design fields follow the framework proposed in Kawamoto et al. (2011) using the Helmholtz PDE filtering and Heaviside projection.

2.1.1. Material density field

In a prescribed, fixed design domain D, a characteristic function χ is defined to describe the material domain Ω_d to be optimized:

$$\chi(\mathbf{x}) = \begin{cases} 0 & \text{for} \quad \forall \mathbf{x} \in D \setminus \Omega_d \\ 1 & \text{for} \quad \forall \mathbf{x} \in \Omega_d \end{cases}, \tag{1}$$

where $\mathbf{x}$ stands for a design point in D and $\chi(\mathbf{x})$ is defined by a scaler function ϕ and the Heaviside function H such that:

$$\chi(\mathbf{x}) = H\left(\phi(\mathbf{x})\right) = \begin{cases} 0 & \text{for} \quad \forall \mathbf{x} \in D \setminus \Omega_d \\ 1 & \text{for} \quad \forall \mathbf{x} \in \Omega_d \end{cases}. \tag{2}$$

To eliminate checkerboard patterns therefore generating mesh-independent results, the Helmholtz PDE filter (Lazarov and Sigmund (2011))is introduced to regularize ϕ:

$$-R_\phi^2 \nabla^2 \tilde{\phi} + \tilde{\phi} = \phi, \tag{3}$$

where R_ϕ is the filter radius, and $\tilde{\phi}$ is the filtered field. Then the density field ρ can be defined by an additional smoothed Heaviside function $\tilde{H}$:

$$\rho = \tilde{H}(\tilde{\phi}). \tag{4}$$

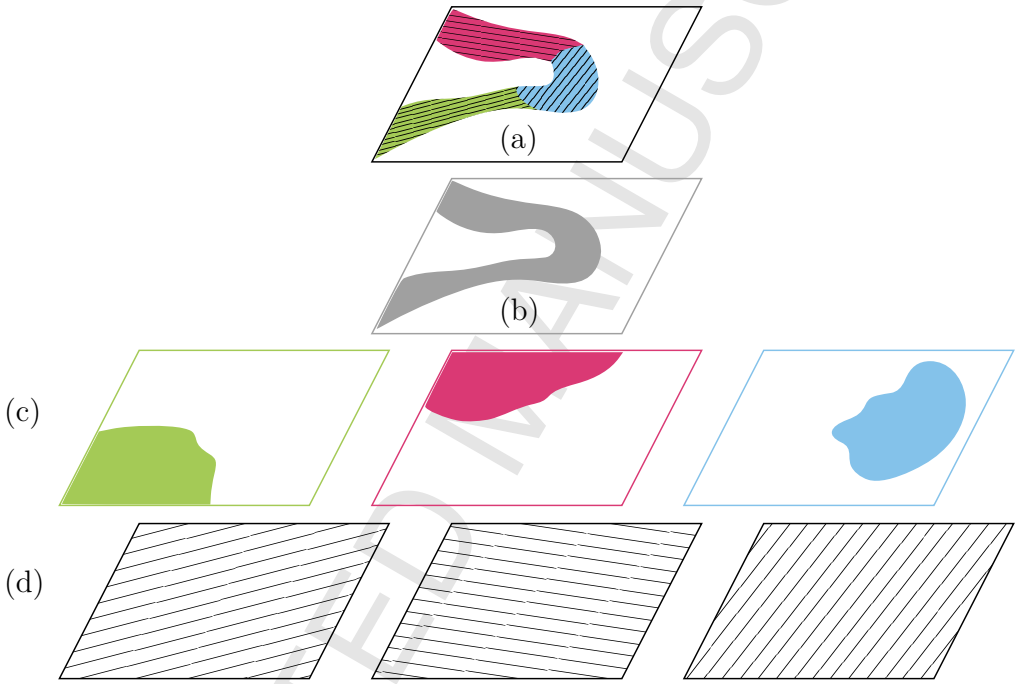

Figure 2: Demonstration of the three-layer design field and the resulting simulation model for an example case of number of components $K = 3$. (a) Simulation model; (b) density field ρ; (c) membership field $m^{(k)}$; (d) orientation field $\vartheta^{(k)}$. (The material orientation for each component can be either unidirectional or curvilinear based on the regularization filter radius used. This figure only shows the unidirectional case.)

After the series of regularization from ϕ to ρ, the resulting density field ρ is bounded between 0 and 1.

2.1.2. Material orientation vector field

Following the Cartesian representation of continuous angles proposed in Nomura et al. (2015), the original material orientation vector field $\upsilon^{(k)} = (\xi^{(k)}, \eta^{(k)})$, bounded by a box constraint $\upsilon^{(k)} \in [-1,1]^D \times [-1,1]^D$ is first regularized by the Helmholtz PDE filter:

$$-\mathbf{R}_\upsilon \nabla^2 \begin{bmatrix} \tilde{\xi}^{(k)} \\ \tilde{\eta}^{(k)} \end{bmatrix} + \begin{bmatrix} \tilde{\xi}^{(k)} \\ \tilde{\eta}^{(k)} \end{bmatrix} = \begin{bmatrix} \xi^{(k)} \\ \eta^{(k)} \end{bmatrix}, \tag{5}$$

where $\mathbf{R}_\upsilon = R_\upsilon^2 \mathbf{I}$, R_υ is the filter radius; $\mathbf{I}$ is an identity matrix; and $\tilde{\upsilon}^{(k)} = (\tilde{\xi}^{(k)}, \tilde{\eta}^{(k)})$ is the filtered orientation field. Then, the (unbounded) $\tilde{\upsilon}^{(k)}$ is projected back to the original box constraint with a smoothed Heaviside function $\tilde{H}$:

$$\bar{\upsilon}^{(k)} = \begin{bmatrix} \bar{\xi}^{(k)} \\ \bar{\eta}^{(k)} \end{bmatrix} = \begin{bmatrix} 2\tilde{H}\big(\tilde{\xi}^{(k)} - 1\big) \\ 2\tilde{H}\big(\tilde{\eta}^{(k)} - 1\big) \end{bmatrix}. \tag{6}$$

As illustrated in Figure 3, the regularized orientation vector field $\bar{\upsilon}^{(k)}$ in a box domain is then projected to a circular domain through an isoparametric projection $\mathbf{N}_c$:

$$\vartheta^{(k)} = \mathbf{N}_c\big(\bar{\upsilon}^{(k)}\big) = \begin{bmatrix} N_{cx}\big(\bar{\xi}^{(k)}, \bar{\eta}^{(k)}\big) \\ N_{cy}\big(\bar{\xi}^{(k)}, \bar{\eta}^{(k)}\big) \end{bmatrix}. \tag{7}$$

where $\vartheta^{(k)} = (\varsigma^{(k)}, \zeta^{(k)})$ is the projected orientation vector field. The transformation from a box domain to a circular domain eliminates the need of the quadratic constraint $\bar{\xi}^{(k)2} + \bar{\eta}^{(k)2} = 1$ for each design point, and ensures singularity-free numerical analyses. For the detailed implementation of the isoparametric projection $\mathbf{N}_c$, readers are referred to Nomura et al. (2015).

By setting different values for R_υ in Equation (5), the maximum allowable curvature of the material orientation in each component k can be explicitly controlled. With a large enough R_υ, the resulting material orientation can be unidirectional.

2.1.3. Component membership vector field

Following the similar regularization scheme as material density and orientation design fields, the original membership vector field $\mu^{(k)}$ is transformed

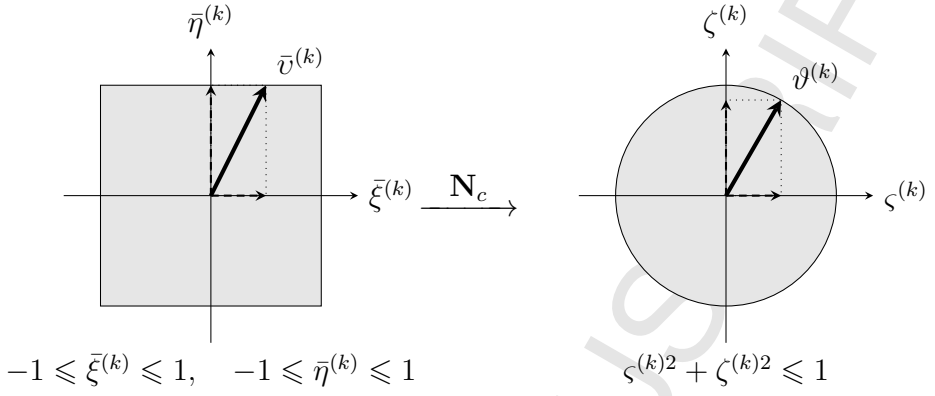

Figure 3: Coordinate transformation for the Cartesian orientation representation through an isoparametric projection scheme.

to $\tilde{\mu}^{(k)}$ and then $\bar{\mu}^{(k)}$ through the Helmholtz PDE filter and smoothed Heaviside projection. For each design point, the resulting $\bar{\boldsymbol{\mu}} = (\bar{\mu}^{(1)}, \bar{\mu}^{(2)}, \cdots, \bar{\mu}^{(K)})$ is bounded by a K-dimensional unit hypercube $[0,1]^K$. As illustrated in Figure 4, the regularized component membership vector field $\bar{\boldsymbol{\mu}}$ in a hypercube domain is then projected to a standard simplex domain through a projection $\mathbf{N}_s$:

$$\mathbf{m} = \mathbf{N}_s(\bar{\boldsymbol{\mu}}) \tag{8}$$

where $\mathbf{m} = (m^{(1)}, m^{(2)}, \cdots, m^{(K)})$ is the projected component membership vector field. The transformation from a hypercube domain to a standard simplex domain eliminates the need of unity constraint $m^{(1)} + m^{(2)} + \cdots + m^{(K)} = 1$ for each design point and ensures singularity-free numerical analyses.

The hypercube-to-simplex projection $\mathbf{N}_s = (N_s^{(1)}, N_s^{(2)}, \cdots, N_s^{(K)})$ is defined as:

$$m^{(k)} = N_s^{(k)}(\bar{\boldsymbol{\mu}}) = \sum_{i=1}^{M} s_i^{(k)} \left\{ (-1)^{(K+\sum_{k=1}^{K} c_i^{(k)})} \prod_{k=1}^{K} (\bar{\mu}^{(k)} + c_i^{(k)} - 1) \right\}, \tag{9}$$

where $M = 2^K$ and $c_i^{(k)} \in \{0, 1\}$ are the number of vertices and the k-th element of the i-th vertex of a K-dimensional unit hypercube, respectively; and $s_i^{(k)}$ is vertex $c_i^{(k)}$ projected to a K-dimensional standard simplex domain,

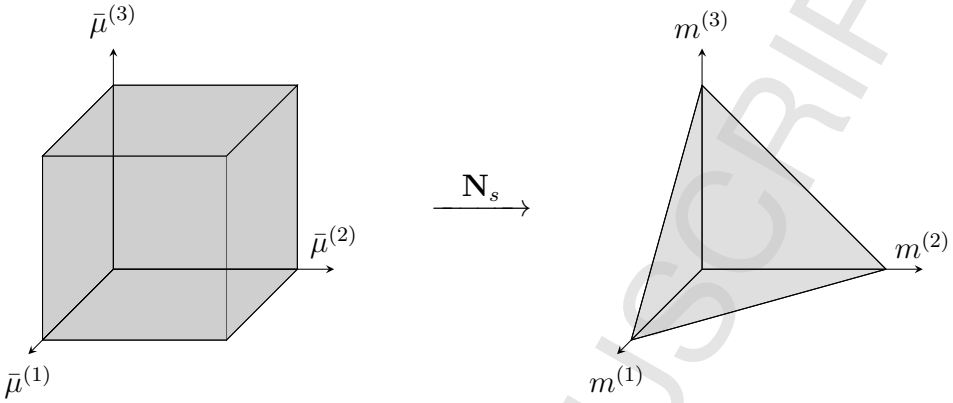

Figure 4: Coordinate transformation for the component membership design field through a K-dimensional hypercube-to-simplex projection for an example case of $K = 3$.

given as:

$$s_i^{(k)} = \begin{cases} \frac{c_i^{(k)}}{\sum_{k=1}^{K} c_i^{(k)}} & \text{if } \sum_{k=1}^{K} c_i^{(k)} \geq 1 \\ 0 & \text{otherwise} \end{cases} . \tag{10}$$

Figure 5 illustrates the projection of sampled points in a unit hypercube using Equations (8)–(10). It can be seen that the evenly distributed points in the hypercube domain are unevenly mapped to the simplex domain. This will lead the projection to favor the points near the center of the simplex at the beginning of optimization. However, due to the penalization parameter P_m introduced later in Equation (11), the optimization will favor convergence to the simplex vertices indicating unique discrete choices of component membership. While the figure shows only for cases $K = 2$ and $K = 3$, the proposed hypercube-to-simplex projection in Equations (8)–(10) works for an arbitrary number of dimensions. It should be noted that the hypercube-to-simplex projection is only applied to the component membership field, and not to the density and orientation fields.

2.2. Elasticity tensor composition

By adopting the multi-phase SIMP-like formulation reported in past literature, the elasticity tensor at each design point can be composed by over-

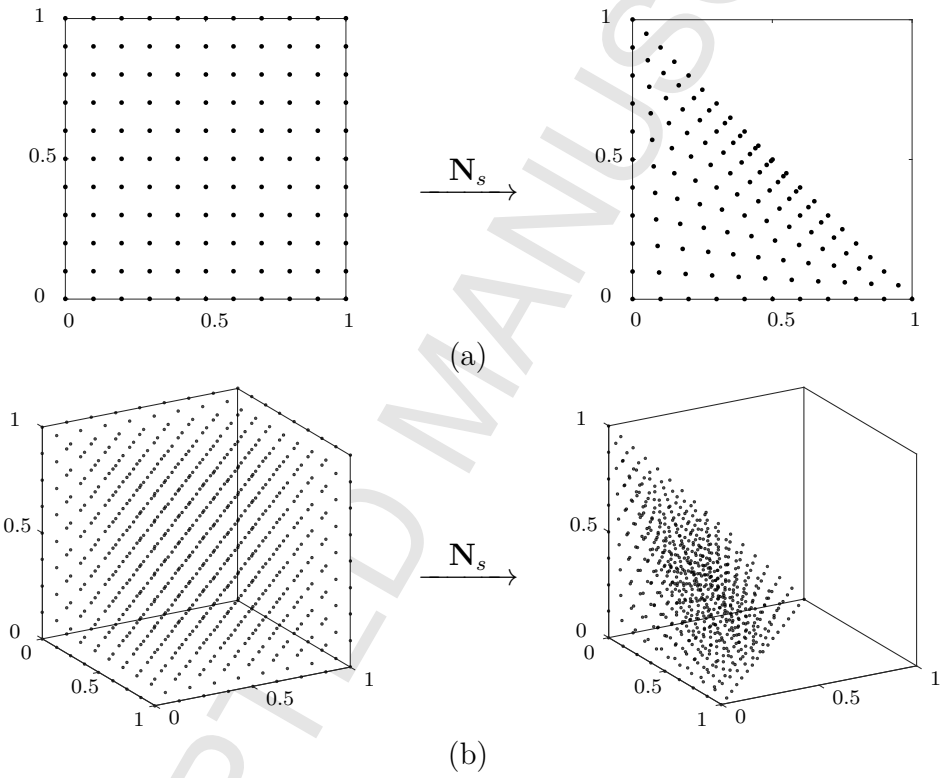

Figure 5: The hypercube-to-simplex projection examples for cases of (a) $K = 2$ and (b) $K = 3$.

laying the elasticity tensor for each component:

$$\mathbf{C} = \rho^{P_d} \sum_{k=1}^{K} \big(m^{(k)}\big)^{P_m} \mathbf{C}^{(k)}, \tag{11}$$

where $\mathbf{C}$ and $\mathbf{C}^{(k)}$ are the composed elasticity tensor and the elasticity tensor for component k, respectively; and P_d and P_m are the penalization parameters for density and component membership, respectively.

This way of composing the elasticity tensor for each phase (component in this case) was considered the simplest choice for multi-phase topology optimization according to Stegmann and Lund (2005). However, it does not satisfy the unity constraint $m^{(1)}+m^{(2)}+\cdots+m^{(K)} = 1$, which allows only one of phase fields (component membership fields in this case) $m^{(k)}$ converging to 1. Rather, Equation (11) often favors all phase fields (component membership fields in this case) $m^{(k)}$ converging to 1, since it would maximize the composed tensor $\mathbf{C}$ with respect to $m^{(k)} \in [0, 1]$. To resolve this issue, different projection methods for phase fields have been proposed. Sigmund and colleagues (Sigmund and Torquato (1997); Gibiansky and Sigmund (2000)) originally proposed a two-phase formulation for topology optimization, which has later been extended to more phases. Stegmann and Lund (2005) proposed another projection scheme, termed the discrete material optimization (DMO). The proposed hypercube-to-simplex projection discussed in Section 2.1.3 can be seen an alternative approach to satisfy the membership unity condition. Through the proposed hypercube-to-simplex projection, the vertices in a unit hypercube that violate the unity condition (*i.e.*, the ones outside of a standard simplex attached to the hypercube) are projected inside of a hypercube and the convergence to them is discouraged by the power law penalization.

By incorporating the material orientation field $\vartheta^{(k)}$ into component elasticity tensor $\mathbf{C}^{(k)}$, the modified composed elasticity tensor $\mathbf{C}$ can be rewritten as:

$$\mathbf{C} = \rho^{P_d} \sum_{k=1}^{K} \big(m^{(k)}\big)^{P_m} \mathbf{C}^{(k)}\big(\vartheta^{(k)}\big), \tag{12}$$

with the transformed anisotropic tensor $\mathbf{C}^{(k)}\big(\vartheta^{(k)}\big)$, given as:

$$\mathbf{C}^{(k)}\big(\vartheta^{(k)}\big) = \mathbf{C}_i + \hat{\mathbf{T}}^{-1}\big(\vartheta^{(k)}\big) \cdot \big(\mathbf{C}_u - \mathbf{C}_i\big) \cdot \hat{\mathbf{T}}'\big(\vartheta^{(k)}\big), \tag{13}$$

where $\mathbf{C}_u$ is a unrotated anisotropic tensor; $\mathbf{C}_i$ is an isotropic component; and $\hat{\mathbf{T}}$ and $\hat{\mathbf{T}}'$ are transformations to rotate a tensor to a direction based on $\vartheta^{(k)}$. For the detailed explanation and derivation of the transformed anisotropic tensor, readers are referred to Nomura et al. (2015).

2.3. Optimization problem

The overall optimization problem of multi-component topology and material orientation design can be stated as follows:

$$\begin{aligned}
\underset{\substack{\phi \\ \mu^{(1)},\cdots,\mu^{(K)} \\ \upsilon^{(1)},\cdots,\upsilon^{(K)}}}{\text{minimize}} \quad & F(\mathbf{u}) \\
\text{subject to} \quad & g_1 := A_d - V^* \leqslant 0 \\
& \phi \in [-1,1]^D \\
& \text{for } k = 1,2,...,K: \\
& g_2^{(k)} := -B^{(k)} + (1-\varepsilon) \leqslant 0 \\
& \mu^{(k)} \in [-1,1]^D \\
& \upsilon^{(k)} \in [-1,1]^D \times [-1,1]^D
\end{aligned} \quad , \tag{14}$$

where $\mathbf{u}$ is the displacement field obtained by solving the static equilibrium equations; $F(\mathbf{u})$ is the objective function for a structural performance; K is the prescribed, maximum allowable number of components; g_1 is the material volume constraint with upper bound V^*; $g_2^{(k)}$ is the constraint to ensure the material anisotropicity for the k-th component with small constant ε; and A_d and $B^{(k)}$ are given as:

$$\begin{aligned}
A_d &= \int_D \rho \, \mathrm{d}\Omega \\
B^{(k)} &= \frac{1}{A_d} \int_D \left\| \vartheta^{(k)} \right\| \mathrm{d}\Omega
\end{aligned} . \tag{15}$$

In the case of the minimization of structural compliance as discussed in the following examples, the objective function can be stated as:

$$F(\mathbf{u}) = \frac{1}{2} \int_D \boldsymbol{\sigma}^T \boldsymbol{\epsilon} \mathrm{d}\Omega, \tag{16}$$

Table 1: Material properties for the numerical examples.

Symbol	Value	Description
E_f	1	Young's modulus of reinforcement material
E_m	1/15	Young's modulus of matrix material
ν_f	0.22	Poisson ratio of reinforcement material
ν_m	0.38	Poisson ratio of matrix material
f_f	0.5	fiber fraction for anisotropic material

and the static equilibrium equations can be stated as:

$$\begin{array}{rcll} -\nabla \cdot \boldsymbol{\sigma} & = & \mathbf{0} & \text{in } D \\ \mathbf{u} & = & \mathbf{0} & \text{on } \Gamma_d \\ \boldsymbol{\sigma} \cdot \mathbf{n} & = & \mathbf{t} & \text{on } \Gamma_n \end{array} , \tag{17}$$

where $\boldsymbol{\sigma} = \mathbf{C} \cdot \boldsymbol{\epsilon}$ is the stress field; $\boldsymbol{\epsilon}$ is the strain field; Γ_d is the Dirichlet boundary defined by zero prescribed displacement; and Γ_n is the Neumann boundary defined by the normal $\mathbf{n}$ and the prescribed traction $\mathbf{t}$.

3. Numerical examples

This section presents several numerical examples in 2D on compliance minimization based on a simplified orthotropic material model per Hull and Clyne (1996):

$$\begin{array}{rcl} E_1 & = & f_f E_f + (1 - f_f) E_m \\ E_2 & = & \{f_f / E_f + (1 - f_f)/E_m\}^{-1} \\ G_{12} & = & \{f_f / G_f + (1 - f_f)/G_m\}^{-1} \\ \nu_{12} & = & f_f \nu_f + (1 - f_f)\nu_m \\ \nu_{21} & = & \{f_f \nu_f + (1 - f_f)\nu_m\} \dfrac{E_2}{E_1} \end{array} . \tag{18}$$

Table 1 summarizes the values of the material properties in Equation (18) used in the numerical examples.

In all examples, the results obtained by the proposed multi-component topology and orientation optimization are compared to the ones by 1) the single-piece topology optimization with an isotropic material using the conventional SIMP method, and 2) the single-piece topology and continuous orientation optimization using Nomura et al. (2015). For the single-piece topology optimization with an isotropic material, the equivalent material

property of randomly orientated discontinuous short fibers are used per Hosford (2013):

$$\begin{aligned} \tilde{E} &= \tfrac{3}{8}E_1 + \tfrac{5}{8}E_2 \\ \tilde{G} &= \tfrac{1}{8}E_1 + \tfrac{1}{4}E_2 \end{aligned} . \tag{19}$$

The nonlinear constrained optimization problem in Equation (14) is solved by the method of moving asymptotes (Svanberg (1987)) with the first derivatives of the objective and constraints. The sensitivity analysis follows the standard adjoint method and is implemented using COMSOL Multiphysics. Interested readers are referred to Olesen et al. (2006) for sensitivity analysis using this software.

The continuation method is applied to the two penalty parameters P_d and P_m, and the anisotropicity constraint parameter ε in Equation (14), based on a fixed continuation and convergence strategy. The density penalty P_d was initialized as 1.5, and updated to 2, 2.5, and 3 at iteration 60, 90, and 120 respectively. The membership penalty P_m was initialized as 1, and updated to 1.5, 2, 2.5, and 3 at iteration 60, 90, 120, and 150 respectively. The anisotropicity constraint parameter ε was initialized as 1, and updated to 0.2, 0.1, and 0.02 at iteration 60, 90, and 120 respectively. The maximum number of iterations was set to 200. Alternative strategies for continuation and convergence can be implemented based on relative measures, *e.g.*, the maximum change in design variables and the first order optimality.

The initial density and component membership were uniformly set to $\rho = V^*$ and $m^{(k)} = 1/K$, respectively. The initial angle $\theta^{(k)}$ for each component k was set to:

$$\theta^{(k)} = (k-1)(180/K)^\circ, \tag{20}$$

where the norm of orientation Cartesian components $\left\| \vartheta^{(k)} \right\|$ was initialized below 0.3, indicating weak initial anisotropicity.

3.1. Single load cantilever example

The proposed method is first applied to a single load cantilever problem. Its design domain D and boundary conditions are presented in Figure 6. The left side of the cantilever is fixed in all degrees of freedom. A unit load is applied at the lower right corner.

A square grid mesh with a side length of 0.02 is used to discretize the design domain D using the Lagrange linear quadrilateral elements. The upper bound for the material volume fraction V^* is set as 0.5. The maximum allowable number of components is set as $K = 3$.

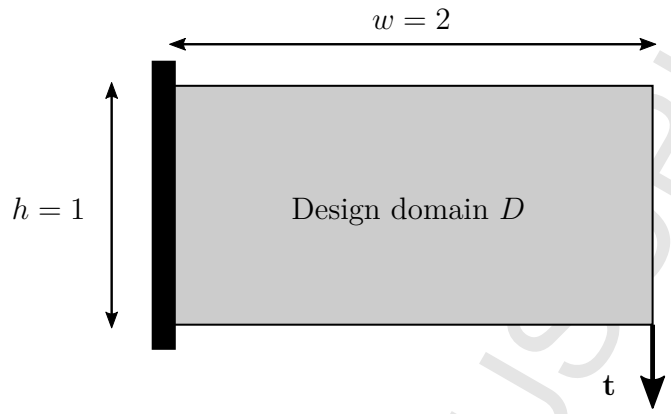

Figure 6: Design domain and boundary conditions for the single load cantilever problem.

3.1.1. Iterative details

Figure 7 shows intermediate multi-component topologies at different iterations during the course of optimization. For each iteration, from left to right, the density field ρ, membership field $m^{(k)}$, component field (product of the two) $\rho m^{(k)}$, and material orientation field $\vartheta^{(k)}$ are shown. The filter radius R_ϑ in Equation (5) is set to a large enough value so the $\vartheta^{(k)}$ can become unidirectional within each component k. The colors of streamlines in orientation plots indicate the state of material anisotropicity levels $\left\|\vartheta^{(k)}\right\|$ based on a color map whose scale is shown in the bottom. As discussed earlier, the optimization was initialized with uniform density and membership distributions. The material anisotropicity levels were initialized as very weak, as seen in Figure 7(a). The component partitioning started happening when the overall topology was not yet clear (Figure 7(b)), and finally converged at iteration 200 (Figure 7(d)). Both the angular values and anisotropicity levels of the optimized orientations are different from their initializations. At the end of optimization in Figure 7(d), only the component membership in the regions of zero density shows some gray, which would have no influence on structural performances. Indeed, after the density and component membership fields are multiplied, the resulting component filed (the third column of Figure 7(d)) have clear crisp boundaries.

To demonstrate the effectiveness of the proposed hypercube-to-simplex projection and penalization scheme, in Figure 8 (from left to right), the component membership field in the hypercube domain $\bar{\mu}^{(k)}$, in the projected sim-

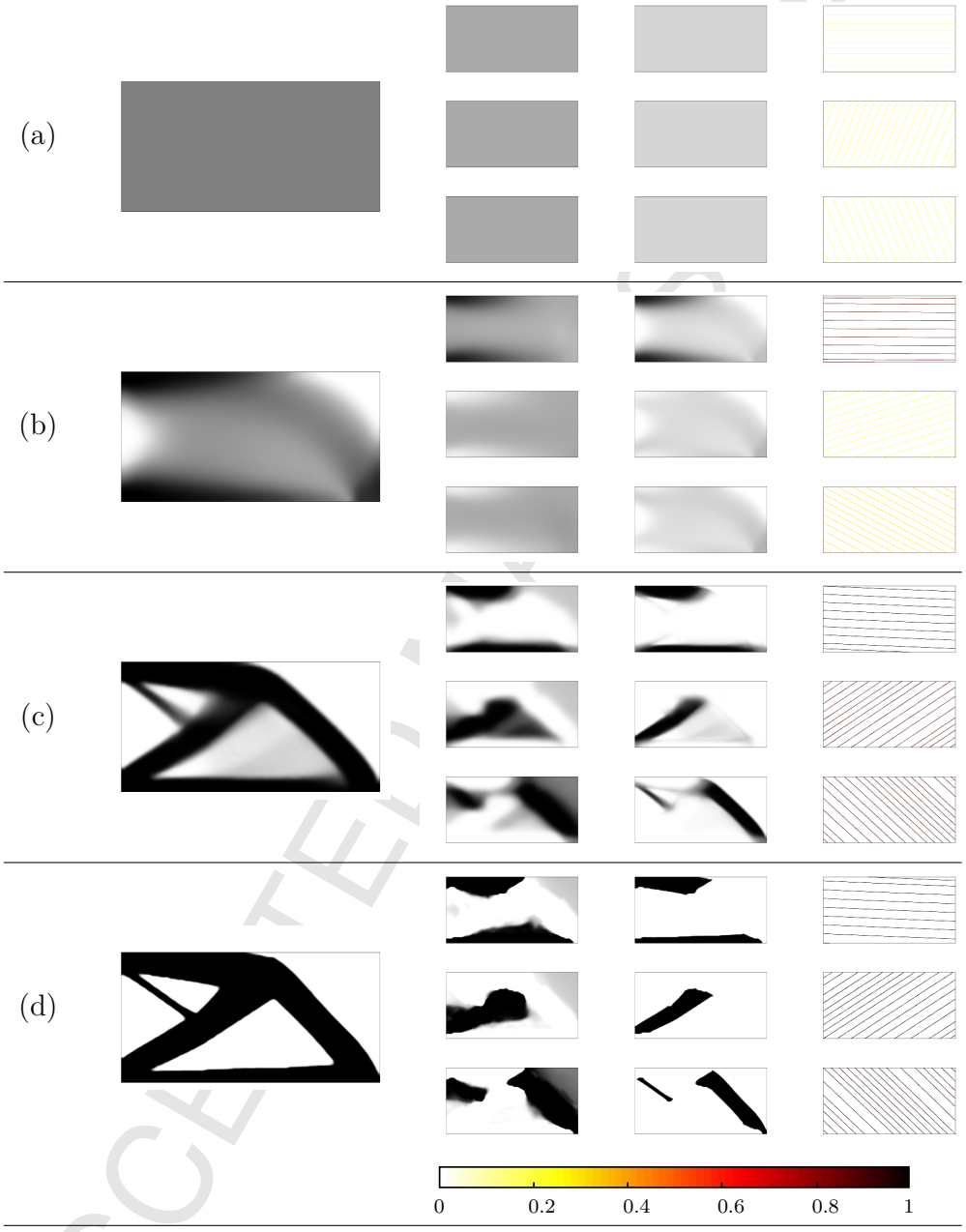

Figure 7: Iterative details of all design fields for the single load cantilever problem with $K = 3$ at (a) iteration 1; (b) iteration 5; (c) iteration 50; and (d) iteration 200. For each iteration, from left to right, the density field ρ, membership field $m^{(k)}$, component field (product of the two) $\rho m^{(k)}$, and material orientation field $\vartheta^{(k)}$ are shown.

plex domain $m^{(k)}$, and in the penalized domain $\rho^{P_d}\left(m^{(k)}\right)^{P_m}$ are visualized at different iterations during the optimization. With the hypercube-to-simplex projection and penalization scheme, undesired vertices in the original hypercube domain that do not satisfy the membership unity constraint have been eliminated. With the continuation on the penalization parameter P_m, the component membership field gradually converged to the three vertices with unique membership selections. The component partitioning at the end of optimization at iteration 200 in Figure 7(d) shows that a unique selection of memberships for each non-void design point is successfully achieved with the proposed hypercube-to-simplex projection and penalization scheme.

The resulting multi-component topology and its component-wise unidirectional orientations are plotted in Figure 9, by visualizing different components with colors. It is clearly seen that the resulting material orientations mostly align the longitudinal directions of beam-like substructures. This supports an empirical knowledge that the optimal material orientation should coincide with the major principal stress direction for compliance minimization problems. The resulting optimized structural compliance is 6.21. While desirable for economical production in large quantities, multi-component structures with component-wise unidirectional orientations like this cannot be obtained by existing continuous orientation methods or discrete orientation methods.

It should be noted that the proposed formulation does not have a constraint to prevent the disconnected pieces in a single component membership, as seen in two isolated pieces for both the green and blue components (substructures) in Figure 9. This is because, for fixed-axis composite layup, ATL, and TFP processes, substructures with an identical (semi-)unidirectional orientation do not have to be physically connected to take advantage of the benefit of (semi-)unidirectional panel/tape/fiber placement. However, imposing such connectivity can be important for other applications, which is left for future research.

The convergence history of the optimization process is plotted in Figure 10. As seen in Figure 10(a), the local fluctuation of the compliance (objective function) was mainly caused by the continuation of the penalization parameters. Otherwise, it was almost monotonically decreasing. As seen in Figure 10(b), the volume constraint remained active throughout the optimization. As seen in Figure 10(c), the membership field also satisfied the unity constraints, because the unity measure $\int_D \rho \|\boldsymbol{m}\| \, \mathrm{d}\Omega \, / A_d$ converged

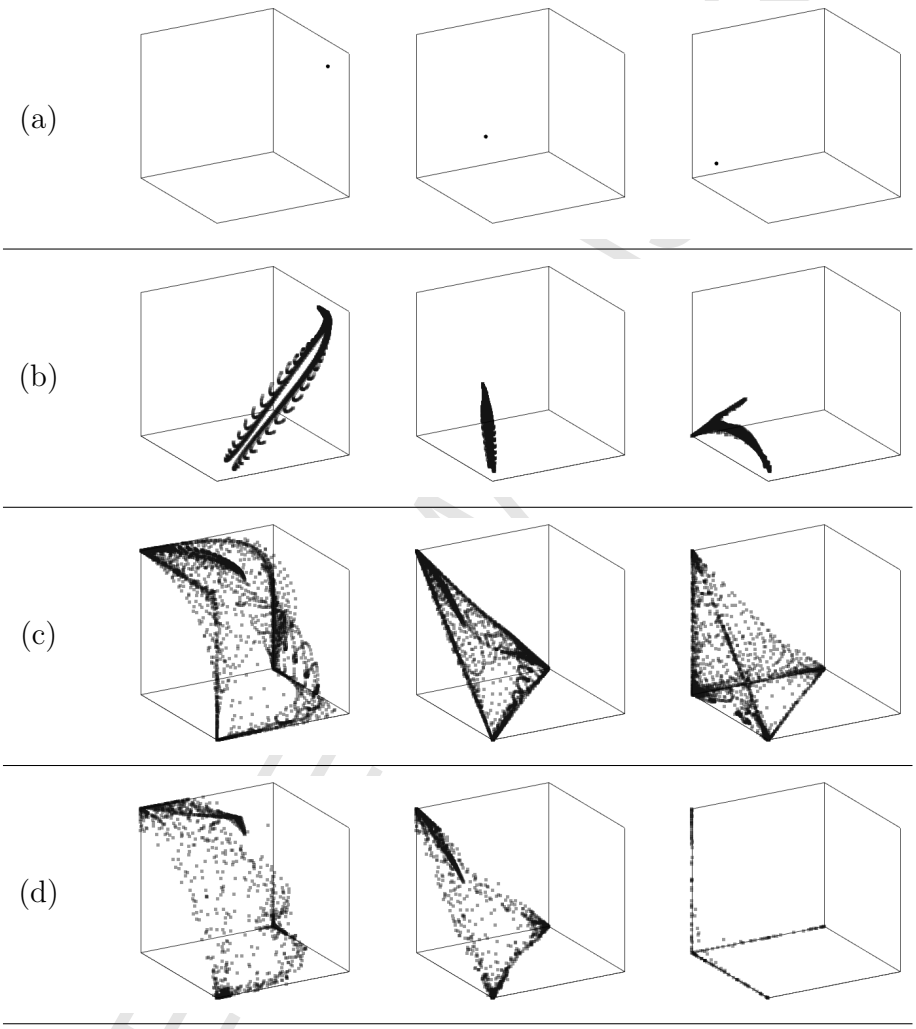

Figure 8: Iterative details for the convergence of component membership field at (a) iteration 1; (b) iteration 5; (c) iteration 50; and (d) iteration 200. Columns show, from left to right, the component membership field in the hypercube domain $\bar{\mu}^{(k)}$, in the projected simplex domain $m^{(k)}$, and in the penalized domain $\rho^{P_d}\big(m^{(k)}\big)^{P_m}$.

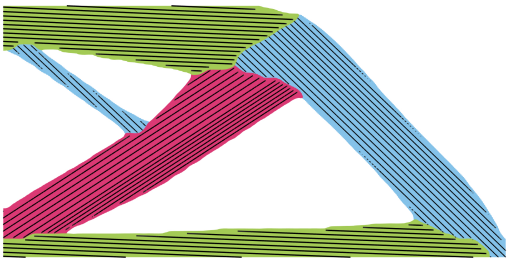

Figure 9: The optimized three-component topology with component-wise unidirectional orientations. Its optimized structural compliance is 6.21.

approximately to 1 at the end of optimization. Thanks to the adopted penalization scheme, the membership unity measure was not necessary as an additional constraint in the optimization problem. It was plotted here just for the monitoring purpose. As seen in Figure 10(d), the material anisotropicity constraints for all components were active at the end of optimization as well.

As a comparison, the optimized single-piece topology with an isotropic material is presented in Figure 11(a) following the assumption of randomly oriented discontinuous short fibers in Equation (19). Its optimized structural compliance is 9.92, inferior to the anisotropic multi-component design. In addition, the optimized single-piece topology with the continuous orientation design is presented in Figure 11(b) following the method proposed in Nomura et al. (2015). As expected, the resulting compliance is 4.07, which is superior than both cases discussed above.

3.1.2. Curvilinear fiber orientation

One way to further improve the performance of multi-component composite structures is to allow curvilinear fiber orientations within each component instead of enforcing unidirectional fiber orientations. By reducing the filter radius on the orientation vector field, one can control the maximum allowable curvature of the fiber orientation within each component. Figure 12(a) presents the optimized three-component topology design allowing a moderate level of curvature on fiber orientations. The structural compliance is improved to 5.65, as opposed to 6.21 in the three-component unidirectional case. Its design fields at the end of optimization are visualized in Figure 12(b–c).

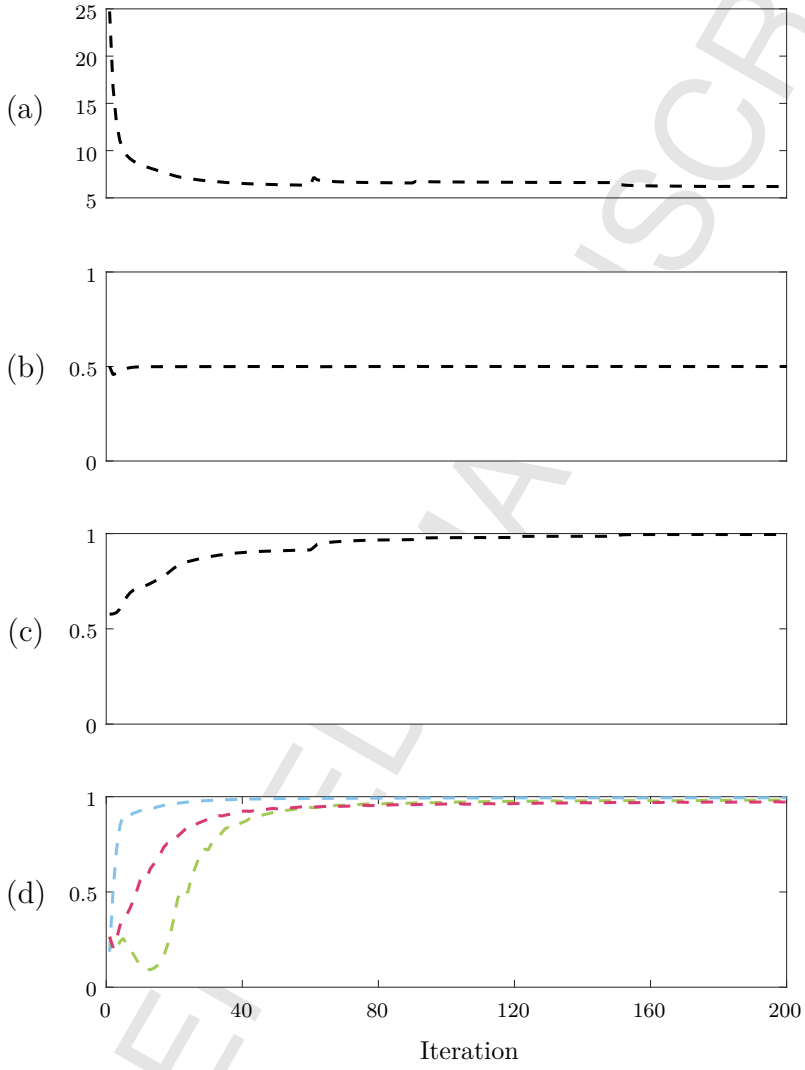

Figure 10: Convergence history for the single load cantilever problem with $K = 3$. (a) Compliance (objective function); (b) volume constraint; (c) membership unity measure; (d) material anisotropicity constraints. (The membership unity measure is plotted for the monitoring purpose, which is not included as a constraint in the optimization.)

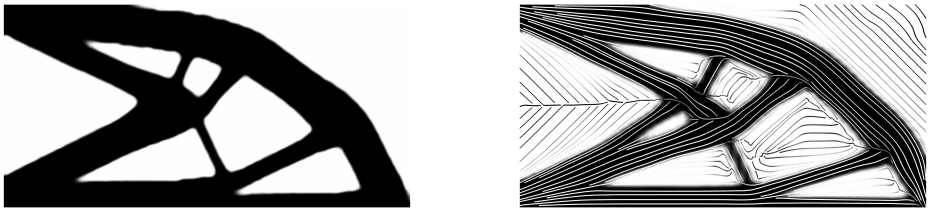

(a) (b)

Figure 11: (a) Optimized single-piece topology with an isotropic material. Its optimized structural compliance is 9.92; (b) optimized single-piece topology with continuous material orientation. Its optimized structural compliance is 4.07.

It is noted that the overall base topology is different from that of the unidirectional case. This is due to the interaction between the density and membership fields with the additional freedom on orientation tailoring. It should also be noted that by allowing curvilinear orientations in composite structures, it is likely that more advanced composite processing techniques are required, which will come with a higher production cost than composite manufacturing processes with unidirectional prepreg preforms.

3.1.3. Different number of components

The maximum allowable number of components K (*i.e.*, the maximum allowable number of discrete orientations), is an input to the optimization. This section discusses the effect of setting different values of K on the optimization results.

Figure 13 shows the optimized multi-component topologies with K equals to 1 to 4. The case of $K = 3$ has been previously presented in Figure 9. The structural compliance improves as the maximum allowable number of discrete orientations increases. Their optimized compliance values are 9.92, 6.76, 6.21, and 5.83 for $K = 1$, $K = 2$, $K = 3$, and $K = 4$ respectively. Similar to the curvilinear study, the overall base topology adapts to different settings of K. It is not surprising to see that with the increase of K, the base topology becomes rather similar to that of the optimized single-piece topology with an isotropic material in Figure 11(a). The similar observation that the base topologies for the anisotropic and isotropic designs are almost identical for single load compliance minimization problems, was also reported

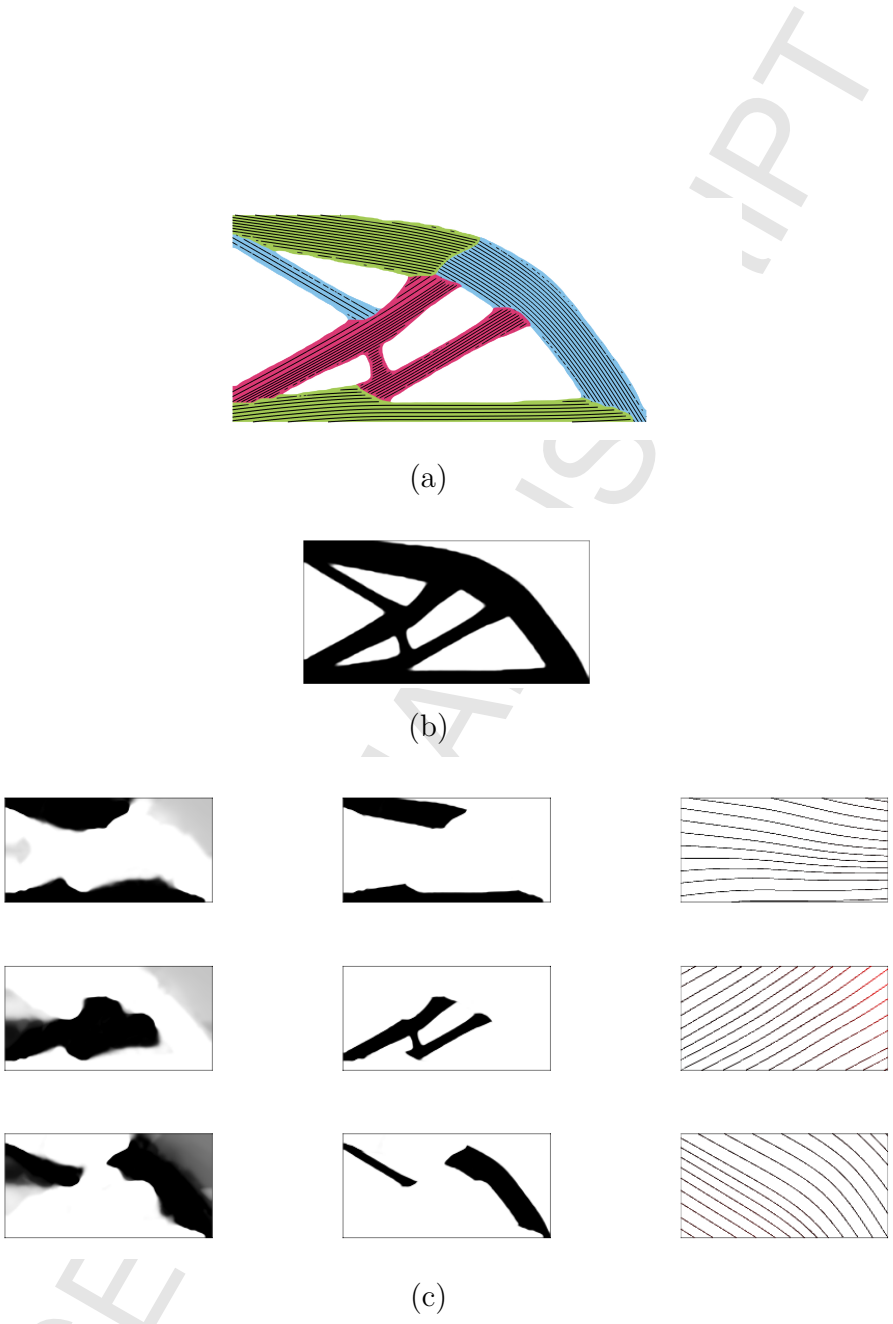

Figure 12: The optimized three-component design allowing component-wise curvilinear orientations. Its optimized structural compliance is 5.65. (a) The optimized multi-component topology; (b) the optimized density field ρ; (c) from left to right: the optimized membership field $m^{(k)}$, the optimized component field (product of the two) $\rho m^{(k)}$, and the optimized material orientation field $\vartheta^{(k)}$.

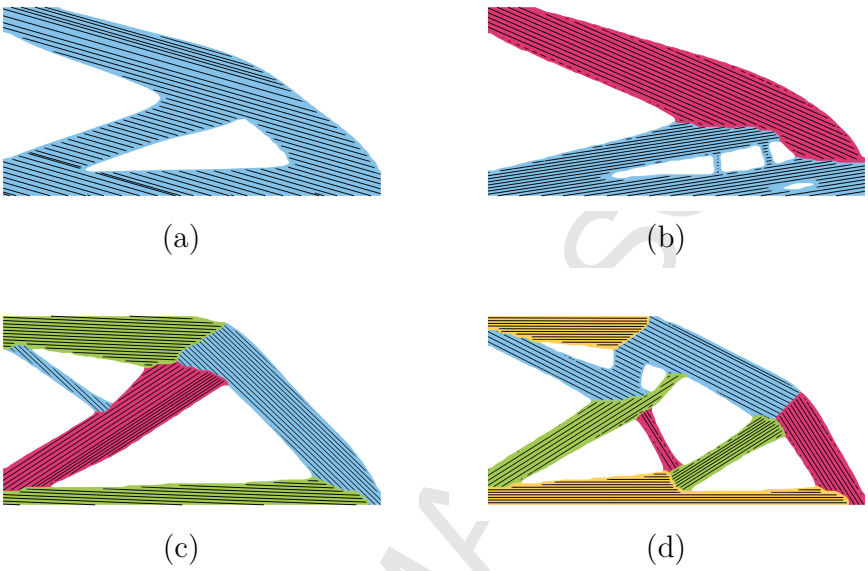

Figure 13: The optimized multi-component topologies with different number of components K settings. (a) $K = 1$; (b) $K = 2$; (c) $K = 3$; (d) $K = 4$.

in Nomura et al. (2015). It can also be seen that as K increases, the multi-component results become closer to the single-piece continuous orientation result in Figure 11(b). While the multi-component results with very large K are expected to become identical to Figure 11(b), such results are not shown since they are not practical for the mass-production composite processes.

In summary, Table 2 compares the optimized structural performances for all numerical examples discussed in Section 3.1. The optimized single-piece topology with an isotropic material, assuming randomly oriented discontinuous short fibers, yields the worst structural performance. The optimized single-piece topology with the continuous material orientation based on Nomura et al. (2015) yields the best structural performance, followed by the optimized multi-component topology with curvilinear material orientations, and then the optimized multi-component topologies with different numbers of unidirectional material orientations.

Though their production costs are not quantitatively modeled, the qualitative estimations are also listed in Table 2, which illustrate the trade-off be-

Table 2: Summary of the structural performance and estimated mass-production cost of cantilever designs discussed in Section 3.1

	Iso-tropic	MTO unidirectional				MTO curv.	Con-tinuous
		$K = 1$	$K = 2$	$K = 3$	$K = 4$		
Com-pliance	9.92	9.27	6.75	6.21	5.83	5.65	4.07
Cost	low	med.	med.	med.	med.	med.+	high

tween structural performance and production cost in large quantities. Among multi-component designs, the fewer number of components (hence orientations) will usually lead to less production cost in large quantities due to the less work for cutting, preforming, and laying-up of composite panels. However, such cost savings would be rather small relative to the high cost of mass-producing single-piece continuous orientation designs, as summarized in Table 2.

3.2. Multi-load tandem bicycle frame example

To demonstrate the applicability of the proposed method to more realistic anisotropic structural design problems, this section presents the design of a tandem bicycle frame. Regular bicycle frame examples have been found in the past literature on topology optimization (Chirehdast et al. (1994); Kumar and Gossard (1996); Zegard and Paulino (2013)). It has served as a good academic example mainly because 1) it has an intuitive structure that everyone is familiar with; 2) it is a simplified 2D problem with only in-plane loading conditions; and 3) it has an irregularly-shaped design domain that requires irregular meshing, which adds some complexity to other examples with a rectangular domain. In addition to these properties, the design of a tandem bicycle frame is inherently a multi-load problem depending on whether the heavier rider is siting in the front or in the rear, which is very suitable for testing anisotropic topology optimization.

Figure 14 shows the design domain and boundary conditions of a simplified tandem bicycle frame example. The design domain is discretized with 11052 free irregular quadrilateral elements. The example assumes that an adult and a child will be riding the bicycle. Depending on who is sitting in the front, there are two loading conditions. Each load is applied and solved independently. The objective for the multi-load problem is formulated as

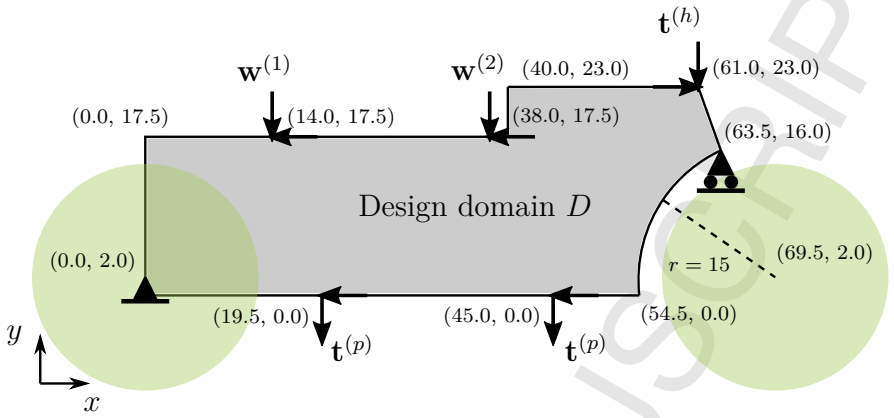

Figure 14: Design domain and boundary conditions for the multi-load tandem bicycle frame example, where $t_x^{(p)} = -1.5$; $t_y^{(p)} = -1.0$; $t_x^{(h)} = 1.0$; $t_y^{(h)} = -1.0$; $w_x = \{-1.0, -0.25\}$; and $w_y = \{-6.0, -1.5\}$. At location $(0.0, 2.0)$, both degrees of freedom in x and y are fixed. At location $(63.5, 16.0)$, only the degree of freedom in y is fixed. The lower left corner of the design domain is set as location $(0.0, 0.0)$.

follows:

$$F_m = F_1 + F_2, \tag{21}$$

where F_m is the multi-load objective function; F_1 and F_2 are structural compliances for the two loading conditions.

Figure 15(a) presents the benchmark isotropic single-piece topology design assuming randomly oriented discontinuous short fibers with a resulting compliance value of 4952. Its deformation plots for the two loading conditions are also presented in Figure 15(b–c). Figure 16(a) presents the optimized multi-component topology with the material orientation design. Its design fields at the end of optimization are presented in Figure 16(b–c). For the anisotropic multi-component topology design, K is set as 3, and the unidirectional fiber orientation is enforced for each component by setting the orientation filter radius larger than the size of the design domain. As we have seen in previous results, the overall base topology is different from that of the isotropic case. The optimized unidirectional fiber orientations mostly align the longitudinal directions of beam-like substructures. The optimized multi-load compliance for the multi-component case is 3312, which is more than 30% improvement over the benchmark isotropic design.

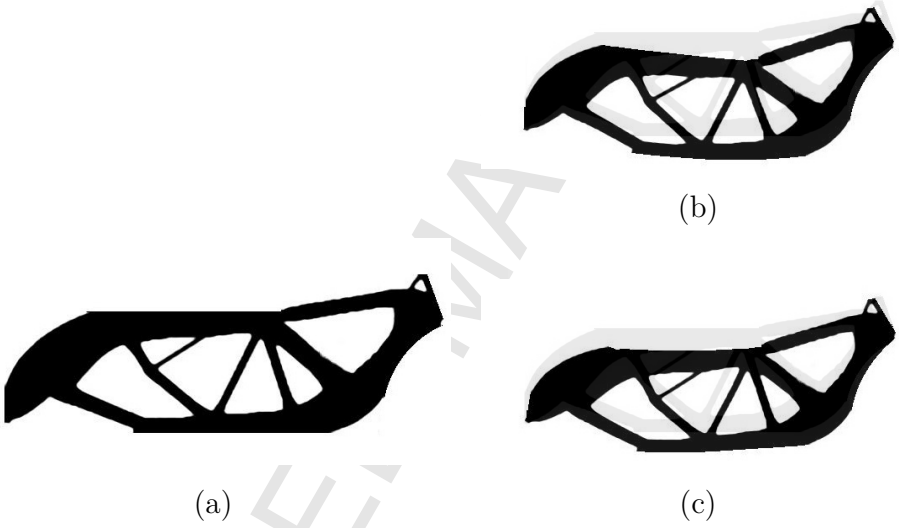

(b)

(a) (c)

Figure 15: (a) The optimized single-piece tandem bicycle frame structure with an isotropic material; (b) the deformed structure under the heavy front loading condition; (c) the deformed structure under the heavy rear loading condition. Its optimized multi-load structural compliance is 4952.

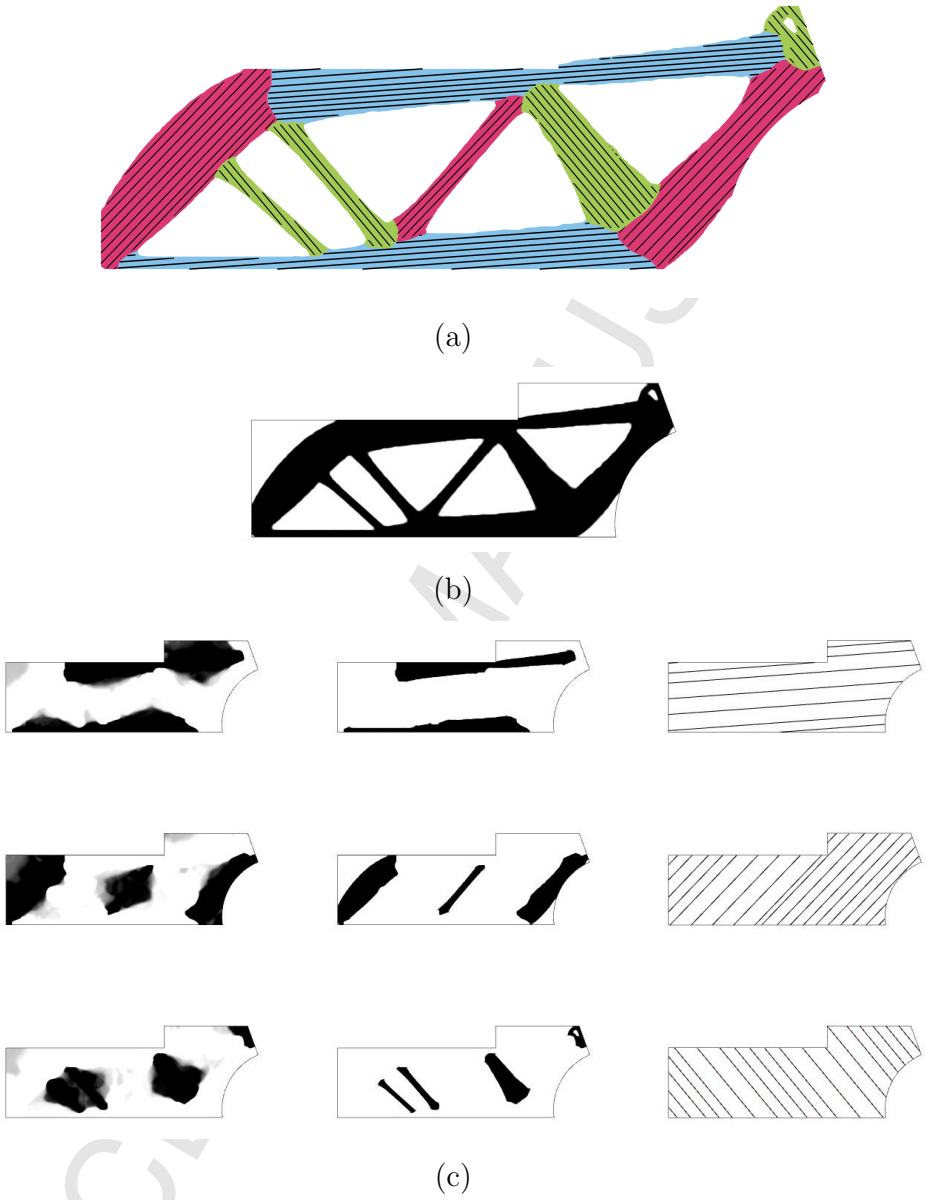

Figure 16: The optimized multi-component tandem bicycle frame structure with component-wise unidirectional material orientations. Its optimized multi-load structural compliance is 3312. (a) The optimized topology; (b) the optimized density field ρ; (c) from left to right: the optimized membership phase field $m^{(k)}$, the optimized component field (product of the two) $\rho m^{(k)}$, and the orientation field $\vartheta^{(k)}$.

4. Conclusion

This paper proposed a topology optimization method for structures made of multiple composite components (substructures) with tailored material orientations. The method was capable of simultaneously optimizing the overall topology, component partitioning, and unidirectional (or curvilinear) material orientation for each component. A vector field variable, similar to the component field variable for multi-material topology optimization, was introduced to represent fractional membership to each component. A hypercube-to-simplex projection and penalization scheme was developed to solve general multi-component topology optimization problems. Through the integration with a continuous material orientation design method (Nomura et al. (2015)), the proposed method was capable of generating multi-component composite structures with tailored material orientations for each component, without a prescribed set of alternative discrete angles. The outcome was a unique composite structural design solution that could not be accomplished by either existing continuous or discrete material orientation methods, and would be most suitable for economical composite manufacturing processes.

The proposed method was applied to several numerical examples. The results were compared to the designs optimized by a conventional single-piece isotropic topology optimization method and a continuous orientation method. The comparison revealed that the proposed method produced unique multi-component topology designs with component-level unidirectional material orientations. The proposed method consistently generated designs with better structural performance than single-piece, isotropic designs. Though the multi-component designs sacrifice on structural compliance compared to the single-piece designs with continuous material orientation, they demonstrated potentially large cost savings in mass production via economical composite manufacturing processes, which require a unidirectional orientation for each component. By allowing the curvilinear orientation in each component, the structural performance of the multi-component designs could be improved, at an expense of less economical, advanced composite manufacturing processes.

The proposed MTO formulation defines one orientation variable for each design point, rather for each component. While it significantly increases the number of orientation design variables, it was chosen due to the flexibility to generalize to curvilinear orientation designs and the marginal increase in computational cost thanks to adjoint sensitivity analysis. In addition, the

formulation does not have a constraint to prevent the disconnected pieces in a single component membership. This is because, for fixed-axis composite layup, ATL, and TFP processes, substructures with an identical (semi-)unidirectional orientation do not have to be physically connected to take advantage of the benefit of (semi-)unidirectional panel/tape/fiber placement. However, imposing such connectivity can be important for other applications, which is left for future research.

Acknowledgment

The funding for this research is provided by Toyota Research Institute of North America (TRINA).

5. Reference

Bendsøe, M. P., 1989. Optimal shape design as a material distribution problem. Structural and Multidisciplinary Optimization 1 (4), 193–202.

Bruyneel, M., 2011. SFP-a new parameterization based on shape functions for optimal material selection: application to conventional composite plies. Structural and Multidisciplinary Optimization 43 (1), 17–27.

Bruyneel, M., Fleury, C., 2002. Composite structures optimization using sequential convex programming. Advances in Engineering Software 33 (7), 697–711.

Chirehdast, M., Gea, H.-C., Kikuchi, N., Papalambros, P., 1994. Structural configuration examples of an integrated optimal design process. Journal of Mechanical Design 116 (4), 997–1004.

Da, D., Cui, X., Long, K., Li, G., 2017. Concurrent topological design of composite structures and the underlying multi-phase materials. Computers & Structures 179, 1–14.

Gao, T., Zhang, W., Duysinx, P., 2012. A bi-value coding parameterization scheme for the discrete optimal orientation design of the composite laminate. International Journal for Numerical Methods in Engineering 91 (1), 98–114.

Gibiansky, L. V., Sigmund, O., 2000. Multiphase composites with extremal bulk modulus. Journal of the Mechanics and Physics of Solids 48 (3), 461–498.

Guirguis, D., Hamza, K., Aly, M., Hegazi, H., Saitou, K., 2015. Multi-objective topology optimization of multi-component continuum structures via a kriging-interpolated level set approach. Structural and Multidisciplinary Optimization 51 (3), 733–748.

Haftka, R. T., Gürdal, Z., 2012. Elements of structural optimization 3rd edition. Vol. 11. Springer Science & Business Media.

Hosford, W. F., 2013. Elementary materials science. ASM International.

Hull, D., Clyne, T., 1996. An introduction to composite materials. Cambridge university press.

Hvejsel, C. F., Lund, E., 2011. Material interpolation schemes for unified topology and multi-material optimization. Structural and Multidisciplinary Optimization 43 (6), 811–825.

Kawamoto, A., Matsumori, T., Yamasaki, S., Nomura, T., Kondoh, T., Nishiwaki, S., 2011. Heaviside projection based topology optimization by a PDE-filtered scalar function. Structural and Multidisciplinary Optimization 44 (1), 19–24.

Kennedy, G. J., Martins, J. R., 2013. A laminate parametrization technique for discrete ply-angle problems with manufacturing constraints. Structural and Multidisciplinary Optimization 48 (2), 379–393.

Kiyono, C., Silva, E., Reddy, J., 2017. A novel fiber optimization method based on normal distribution function with continuously varying fiber path. Composite Structures 160, 503–515.

Kumar, A., Gossard, D., 1996. Synthesis of optimal shape and topology of structures. Journal of Mechanical Design 118, 68–74.

Lazarov, B. S., Sigmund, O., 2011. Filters in topology optimization based on Helmholtz-type differential equations. International Journal for Numerical Methods in Engineering 86 (6), 765–781.

Le Riche, R., Haftka, R. T., 1993. Optimization of laminate stacking sequence for buckling load maximization by genetic algorithm. AIAA journal 31 (5), 951–956.

Lindgaard, E., Lund, E., 2011. Optimization formulations for the maximum nonlinear buckling load of composite structures. Structural and Multidisciplinary Optimization 43 (5), 631–646.

Liu, B., Haftka, R. T., Akgün, M. A., Todoroki, A., 2000. Permutation genetic algorithm for stacking sequence design of composite laminates. Computer Methods in Applied Mechanics and Engineering 186 (2), 357–372.

Liu, J., Ma, Y., 2018. A new multi-material level set topology optimization method with the length scale control capability. Computer Methods in Applied Mechanics and Engineering 329, 444–463.

Lyu, N., Saitou, K., 2005. Topology optimization of multicomponent beam structure via decomposition-based assembly synthesis. Journal of Mechanical Design 127 (2), 170–183.

Nagendra, S., Jestin, D., Gürdal, Z., Haftka, R. T., Watson, L. T., 1996. Improved genetic algorithm for the design of stiffened composite panels. Computers & Structures 58 (3), 543–555.

Niu, B., Olhoff, N., Lund, E., Cheng, G., 2010. Discrete material optimization of vibrating laminated composite plates for minimum sound radiation. International Journal of Solids and Structures 47 (16), 2097–2114.

Nomura, T., Dede, E. M., Lee, J., Yamasaki, S., Matsumori, T., Kawamoto, A., Kikuchi, N., 2015. General topology optimization method with continuous and discrete orientation design using isoparametric projection. International Journal for Numerical Methods in Engineering 101 (8), 571–605.

Olesen, L. H., Okkels, F., Bruus, H., 2006. A high-level programming-language implementation of topology optimization applied to steady-state navier-stokes flow. International Journal for Numerical Methods in Engineering 65 (7), 975–1001.

Pedersen, P., 1989. On optimal orientation of orthotropic materials. Structural Optimization 1 (2), 101–106.

Pedersen, P., 1991. On thickness and orientational design with orthotropic materials. Structural Optimization 3 (2), 69–78.

Rozvany, G. I., 2009. A critical review of established methods of structural topology optimization. Structural and Multidisciplinary Optimization 37 (3), 217–237.

Rozvany, G. I., Zhou, M., Birker, T., 1992. Generalized shape optimization without homogenization. Structural and Multidisciplinary Optimization 4 (3), 250–252.

Sigmund, O., 2001. Design of multiphysics actuators using topology optimization–part ii: Two-material structures. Computer Methods in Applied Mechanics and Engineering 190 (49-50), 6605–6627.

Sigmund, O., 2011. On the usefulness of non-gradient approaches in topology optimization. Structural and Multidisciplinary Optimization 43 (5), 589–596.

Sigmund, O., Torquato, S., 1997. Design of materials with extreme thermal expansion using a three-phase topology optimization method. Journal of the Mechanics and Physics of Solids 45 (6), 1037–1067.

Sørensen, S. N., Lund, E., 2013. Topology and thickness optimization of laminated composites including manufacturing constraints. Structural and Multidisciplinary Optimization 48 (2), 249–265.

Sørensen, S. N., Sørensen, R., Lund, E., 2014. DMTO-a method for discrete material and thickness optimization of laminated composite structures. Structural and Multidisciplinary Optimization 50 (1), 25–47.

Stegmann, J., Lund, E., 2005. Discrete material optimization of general composite shell structures. International Journal for Numerical Methods in Engineering 62 (14), 2009–2027.

Svanberg, K., 1987. The method of moving asymptotes-a new method for structural optimization. International Journal for Numerical Methods in Engineering 24 (2), 359–373.

Thomsen, J., 1992. Topology optimization of structures composed of one or two materials. Structural optimization 5 (1-2), 108–115.

Wang, M. Y., Wang, X., 2004. "Color" level sets: a multi-phase method for structural topology optimization with multiple materials. Computer Methods in Applied Mechanics and Engineering 193 (6), 469–496.

Yildiz, A. R., Saitou, K., 2011. Topology synthesis of multicomponent structural assemblies in continuum domains. Journal of Mechanical Design 133 (1), 011008.

Zegard, T., Paulino, G. H., 2013. Toward GPU accelerated topology optimization on unstructured meshes. Structural and Multidisciplinary Optimization 48 (3), 473–485.

Zhou, Y., Saitou, K., 2017. Gradient-based multi-component topology optimization for additive manufacturing (MTO-A). In: ASME 2017 International Design Engineering Technical Conferences and Computers and Information in Engineering Conference. American Society of Mechanical Engineers.

Zhou, Y., Saitou, K., 2018. Gradient-based multi-component topology optimization for stamped sheet metal assemblies (MTO-S). Structural and Multidisciplinary Optimization 58 (1), 83–94.

Zuo, W., Saitou, K., 2017. Multi-material topology optimization using ordered SIMP interpolation. Structural and Multidisciplinary Optimization 55 (2), 477–491.

1. A new method for optimizing structural topology and material orientation
2. It does not assume a prescribed set of discrete orientations to choose from
3. Output structures are made of components with (semi-)unidirectional orientations
4. Output structures are suitable for economical mass-production processes
5. 2D examples performed comparably to the continuously-curved orientation results